Exact Solutions for Lifting Surfaces

PETER F. JORDAN*
Martin Marietta Laboratories,† Baltimore, Md.

The obstacle which has prevented the determination of exact lifting surface solutions is the singularity at the wing tip. This problem now has been solved analytically for the circular wing and, to an extent, for wings with parabolic wing tips in general. The paper reports the analytical results. Four linearly independent solutions have been determined to very high accuracy and are listed in tables; the tables are brief, since the singularity can be split of. Furthermore, a simplified method is described by which reliable solutions can be calculated quickly if only engineering accuracy is required. The sample solutions given confirm some expected results and provide some unexpected insights into the mechanism of lifting flow.

1. Introduction

VARIOUS numerical methods are available for calculating pressure distributions over lifting wings of finite aspect ratio. Nevertheless, the state-of-the-art is not quite satisfactory. We consider here a very basic engineering model: the thin lifting surface in steady, linear subsonic, and, hence, by the Prandtl-Glauert transformation, incompressible flow. No exact solution for any problem of this type has been available.

Current numerical methods for dealing with such engineering models are approximate methods; they are collocation methods of one type or the other. In cases of discrepancies between numerical prediction and experiment, no reliable criterion has been available for determining the cause. A natural tendency is to blame the simplifications in the model; on the other hand, divergencies in a given numerical method and discrepancies between different methods do occur. Hence there is a definite need for reliable solutions.

The purposes of this paper is to make some such solutions readily available. This is achieved on the basis of an analytical formulation which has been available since 1937. At that time, Prandtl had pointed out that the then new acceleration potential approach would permit one to obtain exact solutions (no a priori assumption about the shape of the trailing wake is involved). The circular wing in incompressible flow appeared to be a suitable model. Kinner[1] formulated the analysis, and he succeeded in determining total lift and total moment. However, the Kinner results for the pressure distribution appear to diverge toward the wing tips.

The key difficulty with any analytical approach (several variations of the Kinner approach exist) lies in the fact that complicated pressure singularities arise at the tips of lifting surfaces. At the same time, and for the same reason, collocation results are particularly unreliable at and near the tips. The engineer wants to know the magnitude and the extent of the numerical error.

Another reason the Kinner formulation had not been examined further was its apparent cumbersomeness. However, we discovered that it can be written in a much simpler form, facilitating a derivation of the analytical structure for the tip singularity at the circular wing. Kinner represents the pressure distribution by an infinite set of coefficients $C_{2\kappa}$; we have derived the formula for the leading elements (sets) in the set $C_{2\kappa}$. These leading elementary sets describe the tip singularity, a rather interesting transition from infinite pressure at the leading edge to zero pressure at the trailing edge. The same singularity occurs on all wing tips of parabolic planform (e.g., on the semi-infinite parabolic wing as well as on a slender elliptic wing). Therefore, to some extent, our analytical results can be generalized.

With regard to the circular wing, our analytical solution is complete: it comprises all those elementary sets of $C_{2\kappa}$ that converge to zero (as $\kappa \to \infty$) more slowly than the difference between different solutions. Of course, the latter must be determined numerically for each given downwash $w(y)$. However, the simpler formulation and the knowledge of the leading sets combine to make such calculations routine.

The analysis which led to our formula is reported elsewhere.[2-5] Incomplete results[2] were used[3] to calculate the initial shape of the wake (and to indicate corrections to earlier analyses of vortex roll-up). The complete solution is described in Ref. 4; certain results of more general mathematical interest are presented in Ref. 5. The purpose of Ref. 6 is to present sample numerical solutions and details of the numerical approach. The present paper is an abbreviated version of Ref. 6.

The relevant analytical results are reported in Sec. 2. Numerical methods and results are discussed in Sec. 3. The planar circular wing, Table 3, is used as the reference problem; additional very accurate solutions are listed in Table 4. This high degree of accuracy required extrapolations, but, for ordinary purposes, it is sufficient to use the solution of a truncated linear system.

Analytical and physical implications of the sample results are discussed in Sec. 4. Section 5 describes a very quick approximate method which is particularly useful if one is interested in details of the pressure distribution over the inner part of the wing.

The singularity at a parabolic wing tip had been one of the unresolved fundamental problems of potential flow theory. The methods presented here are useful beyond this academic point; they allow one to obtain reliable solutions with relative ease. Such solutions can be used to check the accuracy of collocation methods (e.g., Fig. 4) and can provide, sometimes by means of a very brief and straightforward calculation (e.g., Fig. 7) insight into the mechanism of lifting flow which would be difficult and cumbersome to derive convincingly by means of collocation analyses.

2. Analytical Results

a. Pressure Distribution

We describe the pressure difference p between lower and upper wing surfaces by a nondimensional pressure function $\bar{p}$. From $\bar{p}$ the singularities in p, of orders $-\frac{1}{2}$ at the leading edge (l.e.) and $+\frac{1}{2}$ at the trailing edge (t.e.), have been removed

$$\bar{p} = (1-\xi^2)^{1/2} p/q \tag{1}$$

Presented as Paper 71-10 at the AIAA 9th Aerospace Sciences Meeting, New York, January 25–27, 1971; submitted August 18, 1972; revision received March 12, 1973. Research reported here was supported by the Air Force Office of Scientific Research (AFSC), U.S. Air Force, under Contract F44620-69-C-0096.

Index category: Airplane and Component Aerodynamics.

* Principal Research Scientist. Associate Fellow AIAA.

† Formerly RIAS.

Table 1 Comparison of the two limit cases

	$\bar{p}(\xi)$	C_l	ξ_l
2-D	$4(1-\xi)$	2π	-0.5
s.w.	$\left\{\begin{matrix}4k\lvert\xi\rvert \\ 0\end{matrix}\right\}$ if $\left\{\begin{matrix}\xi \leqq 0 \\ \xi \geqq 0\end{matrix}\right\}$	$2k$	$-\pi/4$

Here q is the dynamic pressure, and ξ is the local chordwise coordinate such that $\xi_{\text{l.e.}} = -1$, $\xi_{\text{t.e.}} = +1$ (the notation is shown in Fig. 1).

The given boundary condition is the downwash wV on the wing. V is the forward speed, w the local incidence. Consider the two limit cases for which solutions are known, the infinite uniform wing (2-D; the two-dimensional case) and the slender wing (s.w.)—specifically here, the elliptic s.w. in the limit $k \to 0$, where k is the axis ratio of the ellipse. The nature of the chordwise distribution $\bar{p}(\xi)$ differs distinctly between these two limits. Assume w constant, and normalize to $w = 1$. A comparison is shown in Table 1 where C_l is the local lift coefficient, and ξ_l is the local center of pressure.

In 2-D, $\bar{p}(\xi)$ is a polynomial of order $(n+1)$ in ξ if $w(\xi)$ is a polynomial of order n. Such smooth distributions $\bar{p}(\xi)$ we call 2-D type distributions. In contrast, the s.w. distribution has a kink at the wing axis $\xi = 0$.

On a wing with finite aspect ratio and with rounded (parabolic) tips, 2-D type distributions must prevail over the inner part of the wing span but the kinked s.w. type must exist at the tip point. Indeed, this is confirmed by the exact solution. The latter is derived from the following expression for the pressure function $\bar{p}$:

$$\bar{p}(r,\phi)\bar{y}/4 = \sum_{\kappa=0}^{\infty} C_{2\kappa} r^{2\kappa} \cos 2\kappa\phi + \sum_{\lambda=0}^{\infty} C_{2\lambda+1} r^{2\lambda+1} \sin(2\lambda+1)\phi \tag{2}$$

Each sum on the right is a power series in r and simultaneously a Fourier series in the angle ϕ. The coefficients C_n are the unknowns.

The expression (2) has been derived from the formulation of Kinner[1] under the assumption that the given downwash on the wing is both symmetrical and without camber‡

$$w(\xi, y) = w(y) = w(-y)$$

The function $\bar{p}$ is subject to the Kutta condition

$$\bar{p}_{\text{t.e.}} \equiv \bar{p}(1, -\pi < \phi < 0) \equiv 0 \tag{2a}$$

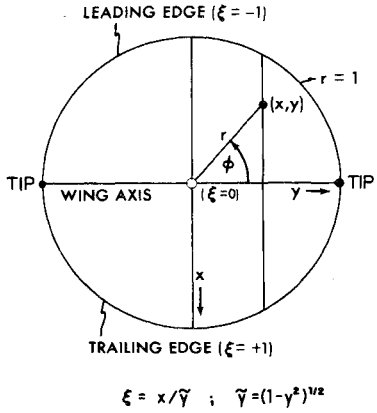

Fig. 1 Coordinates and notation.

‡ Our notation differs somewhat from that of Kinner.[1] The analysis can be rewritten readily if $w(y)$ is antisymmetric; the tip singularity will not be different. Kinner[1] discusses also wings with camber; for this case, the tip singularity has not been investigated rigorously, but it seems that finite camber will not affect its nature.

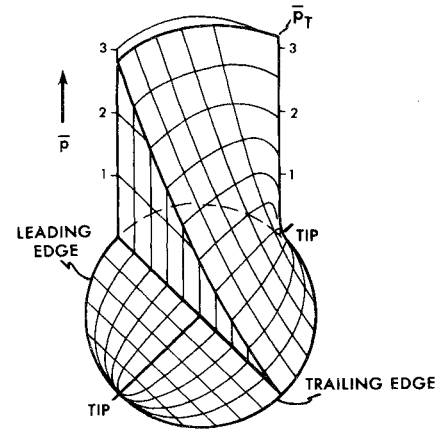

Fig. 2 Relief of pressure function over one-half of planar wing.

and to the condition that its induced downwash must equal $w(y)$.

Chordwise integration of (2) yields the local lift coefficient

$$C_l(y) = \left(\frac{2\pi}{\bar{y}}\right) \sum_{\kappa=0}^{\infty} C_{2\kappa} P_{2\kappa}(y) \tag{3a}$$

and the local moment coefficient

$$\xi_l(y) C_l(y) = -\pi \sum_{\lambda=0}^{\infty} (2\lambda+1) C_{2\lambda+1} \bar{P}_{2\lambda}(y) \tag{3b}$$

The $P_{2\kappa}$ are the Legendre polynomials, the $\bar{P}_{2\lambda}$ their derivatives (respectively, the ultraspherical or Gegenbauer polynomials)

$$\bar{P}_{2\lambda} = [1/(\lambda+1)(2\lambda+1)](d/dy) P_{2\lambda+1}(y) \tag{3c}$$

Both are symmetrical and orthogonal, normalized such that

$$P_{2\kappa}(\pm 1) = \bar{P}_{2\lambda}(\pm 1) = 1 \text{ for all } \kappa \text{ and } \lambda \tag{3d}$$

Additional spanwise integration yields total lift coefficient and center of pressure

$$C_L = 8C_0; \quad \xi_L = -C_1/3C_0 \tag{3e}$$

They are given by the first two coefficients alone.

The pressure function $\bar{p}$ has to fulfill the Kutta condition, and its induced downwash $w_i(y)$ must equal the given downwash $w(y)$. The latter is always regular at the tips, and thus $w_i(y)$ must be regular. These two conditions enforce a specific tip singularity in $\bar{p}$. Before we list the analytical formulas for this singularity, let us review its graphical presentations, Figs. 2–4. These graphs apply to our reference case, the planar wing, normalized to $w(y) \equiv 1$.

Shown in Fig. 2 is a relief of $\bar{p}$ over the right half-wing. Noting the prediction of both lifting line theory (large span) and s.w. theory (small span) that the lift distribution over planar elliptic wings is an ellipse, and assuming that this prediction would hold for all elliptic wings, we would have $C_l = \text{const} = C_L = 1.790\ldots$ in Fig. 2. Using rounded-off numbers, we would thus expect $\bar{p}_{\text{t.e.}} = 4C_L/\pi = 2.28$ from 2-D in Table 1. The actual $\bar{p}_{\text{t.e.}}$ curve in Fig. 2 lies somewhat higher; this is due, mainly, to the fact that the chordwise distributions $\bar{p}(\xi)$ are not linear (as in Table 3) but are concave curves. However, they are 2-D type curves, as expected, over the inner part of the wing span.

For the wing tip, we should have $\bar{p}_{\text{l.e., tip}} = \bar{p}_T = 2C_L = 3.58$ from s.w. in Table 1. The actual value in Fig. 2 is $\bar{p}_T = 3.19$. That this value is distinctly smaller than predicted is not a failure of s.w. theory. Rather, it turns out, see Fig. 4, that the correct lift distribution over planar elliptic wings is not an ellipse (this was already likely from Ref. 1).

Additional information about the transition to the tip is provided by the curve for ξ_l, Fig. 3. Over most of the span, ξ_l is not much forward of the $\frac{1}{4}$-chord point $\xi = -0.5$, see 2-D in Table 1. The transition to the tip value $-\pi/4$ (see s.w. in Table 1) occurs rapidly and with a vertical tangent.

The amplitude $\bar{p}_T$ of the tip singularity is given by

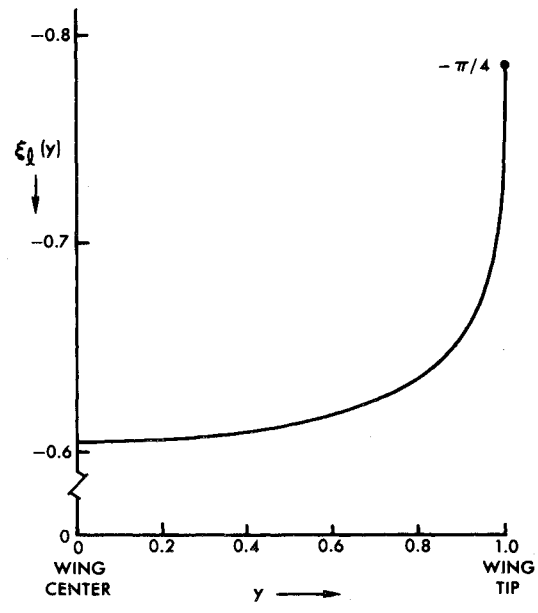

Fig. 3 Chordwise position of center of pressure.

$$\bar{p}_T \equiv \lim_{\phi \to +0} \bar{p}(1,\phi) = 8 \sum_{\lambda=0}^{\infty} (2\lambda+1) C_{2\lambda+1} \tag{4}$$

Moving toward the tip along any half-ellipse $\xi = \text{const}$, one reaches

$$\lim_{y \to 1} \bar{p}_{(\xi=\text{const})} = \begin{Bmatrix} |\xi| \bar{p}_T \\ 0 \end{Bmatrix} \text{ if } \begin{Bmatrix} \xi \leqq 0 \\ \xi \geqq 0 \end{Bmatrix} \tag{4a}$$

This is in agreement wth the s.w. distribution $\bar{p}(\xi)$ in Table 1. However, on a wing of finite span, this kinked distribution is confined to the tip point itself, as illustrated by Figs. 2 and 3. Note from Table 1 that Eq. (4a) implies $C_l(1) = p_T/2$.

Another consequence of the Kutta condition is that the sum of all coefficients $C_{2\kappa}$ is zero

$$\sum_{\kappa=0}^{\infty} C_{2\kappa} = 0 \tag{5}$$

and that the two sets of coefficients are fully interdependent (equivalent to each other). They obey the reversible transformation

$$\pi C_{2\lambda+1} = 2 \sum_{\kappa=0}^{\infty} \frac{\bar{\lambda} C_{2\kappa}}{\bar{\lambda}^2 - \kappa^2} \qquad \text{(all } \lambda\text{)} \tag{6a}$$

$$\pi C_{2\kappa} = 2 \sum_{\lambda=0}^{\infty} \frac{\bar{\lambda} C_{2\lambda+1}}{\bar{\lambda}^2 - \kappa^2} \qquad \text{(times } \tfrac{1}{2} \text{ if } \kappa = 0\text{)} \tag{6b}$$

where $\bar{\lambda} \equiv (\lambda + \frac{1}{2})$. The result of applying the operator (6b) to a suitable set $C_{2\lambda+1}$ automatically fulfills the zero sum condition (5).

Because of the interrelation (6a, b), one needs only one of the two sets of coefficients. From the remark that the given downwash $w(y)$ is always regular at the wing tips arises the following formula for the set $C_{2\kappa}$:

$$-C_{2\kappa} = \left[\frac{4}{\kappa(4\kappa+1)} - \frac{3 \log^2 \kappa}{16\pi^2 \kappa^4} \right] a_2 + R_\kappa \qquad (\kappa \neq 0) \tag{7}$$

In Eq. (7), the number a_2 represents the amplitude of the tip singularity

$$a_2 = \bar{p}_T/8\pi = C_l(1)/4\pi \tag{8}$$

and the expression in brackets is a general formula for the leading term; it describes the dominant analytical structure of the tip singularity. The set R_κ is called the remainder set; it is $O(\kappa^{-4} \log \kappa)$ and differs from solution to solution.

Clearly (7) is meaningless for $\kappa = 0$; the leading coefficient C_0 is determined by (5). Because of this, it is convenient to specify that the set $C_{2\kappa}$ is built up from elementary sets, denoted by E_κ, which individually fulfill (5). Particularly useful are the "rational" sets§

$$E_0{}^r = \zeta(r); \quad E_\kappa{}^r = -\kappa^{-r} \qquad (\kappa \neq 0) \tag{9}$$

because for the two leading sets in Eq. (7), $E_\kappa{}^2$ and $E_\kappa{}^3$, one can derive certain analytical results. In the present section, we are concerned with the pressure distribution. Let $\bar{p}_r$ be the pressure function $\bar{p}$ which arises from inserting the set $E_\kappa{}^r$ into (6a) to determine its corresponding set $C_{2\lambda+1}{}^r$ and inserting both sets into (2). Only $\bar{p}_2$ has a finite tip value $\bar{p}_T$. For all higher r (and, in fact, for all sets which converge faster than the set $E_\kappa{}^2$) we have $\bar{p}_T = 0$. Thus $\bar{p}_2$ alone already describes the most important part of the tip singularity.

For $\bar{p}_2$ we have the following analytical result:

$$\begin{aligned} \bar{p}_{2,\text{l.e.}} &= \frac{8\phi}{\sin\phi}(\pi - \phi) \\ \bar{p}_{2,\text{axis}} &= 4[\zeta(2) - f(\tilde{y}^2)]/\tilde{y} \\ &\sim 4\tilde{y}[2\log(1/\tilde{y}) + 1 + \tilde{y}^2 \log(1/\tilde{y}) + \cdots] \end{aligned} \tag{10}$$

The function f here is the dilogarithm, (see, e.g., 27.7 of Ref. 7). The two results of Eqs. (10) exhibit the characteristic properties of $\bar{p}$ in Fig. 2: a smooth curve along the l.e. and a vertical tangent at the tip in $\bar{p}_{\text{axis}}$.

The analytical result (10) is useful because the process of calculating $\bar{p}$ numerically by summing the series (2) deteriorates on approaching the wing tip. Note in particular the factor $\tilde{y}$ on the left of (2) which goes to zero at the tip. The difficulty is most pronounced along the wing axis; here one can match numerical results for the inner part of the wing with the analytical result (10) that dominates near the tip.

We complement (7) by noting the asymptotic behavior of the set $C_{2\lambda+1}$:

$$C_{2\lambda+1} \sim a_2 \log\lambda/2\pi\lambda^3 + 0(1/\lambda^3) \tag{11}$$

Here again, the leading elementary set has the factor a_2, but the amplitude of the next set differs from solution to solution.

b. Lift Distribution

The local lift coefficient is given by (3a). In order to evaluate the consequences of (7) on the lift distribution, we would like to know the functions $e(y)$ created by the elementary sets in (7)

$$e(y) = \sum_{\kappa=0}^{\infty} E_\kappa P_{2\kappa}(y) \tag{12}$$

We have analytical results only for the two leading sets $E_\kappa{}^r$

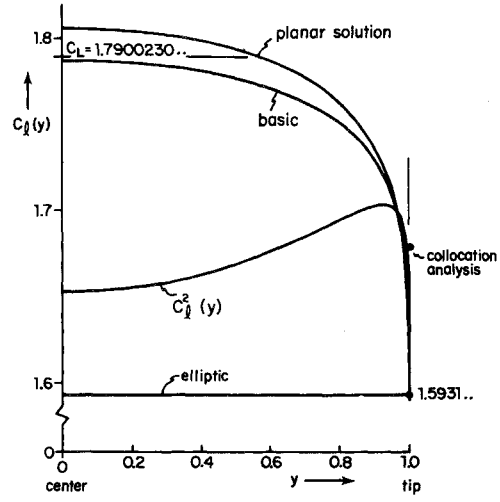

Fig. 4 Lift coefficient over planar wing.

§ Here ζ denotes the Rieman function; see, e.g., Tables 23.3 of Ref. 7.

$$e_2(y) = 2\tilde{y}+\tfrac{1}{2}\tilde{y}^2\log(2/\tilde{y})+O(\tilde{y}^2)$$
$$e_3(y) = \tilde{y}^2\log(2/\tilde{y})+O(\tilde{y}^2) \qquad (13)$$

Using these, we obtain

$$C_l(y) = [1+(\tfrac{1}{8})\tilde{y}\log(2/\tilde{y})]C_l(1)+O(\tilde{y}) \qquad (14)$$

The significance of the logarithmic term in (14) is illustrated by Fig. 4. Our reference solution is shown. An elliptic lift distribution is represented by a horizontal line in Fig. 4. Such a lift distribution produces a positive infinite downwash on the wing at the tip. The curve $C_l{}^2(y)$ represents the contribution of the set $E_\kappa{}^2$; its logarithmic part is too large [according to Eqs. (13)], and it overshoots the correct solution near the tip. Its downwash is negative infinite at the tip. The curve labeled "basic," composed of the first three rational sets ($r = 2$, 3, and 4) such that its downwash is finite (though not regular) at the tip, approaches the correct solution asymptotically. Most significant is that the correct solution has a vertical tip tangent: this has a pronounced effect on the downwash directly behind the wing.[3]

Collocation methods generally assume an "elliptic type" of lift distribution, a distribution to which, in Fig. 4, corresponds a curve with a finite tip tangent. The point marked "collocation analysis" in Fig. 4 is the result of a method[8] characterized by unusually careful integration procedures. Its result[8] coincides with the correct planar curve over the inner part of the wing span, but it deviates at the tip by 5.4%.

As in the case of (10), we note that the analytical result (14) is needed for matching with numerical results; summation according to (3a) deteriorates on approaching the tip. Since the dominant features of the tip singularity are independent of the wing planform away from the tip, the result (14) can be generalized to apply to any wing with parabolic tips. The characteristic length for describing the tip singularity is the tip radius of the wing planform. Let r be this radius and b the wing span. In order to generalize (14), one simply substitutes $\tilde{y}(b/2r)$ for $\tilde{y}$. [The same substitution in Eq. (10) yields the dominant term $\bar{p}_{\text{axis}}$ for arbitrary wings.]

c. Downwash Equations

The given downwash $w(y)$ can be described by a set of downwash coefficients w_s

$$w_s = (4s+3)\int_0^1 \left\{\int_0^y w(\eta)\,d\eta\right\} P_{2s+1}(y)\,dy \qquad (15)$$

Here P denotes the Legendre polynomial. Reversing (15), one finds

$$w(y) = \sum_{s=0}^{\infty}(s+1)(2s+1)w_s\bar{P}_{2s}(y) \qquad (15a)$$

where the $\bar{P}_{2s}(y)$ are the Gegenbauer polynomials of (3c) and are subject to normalization (3d).

In our reference problem,

$$w_0 = 1; \quad w_{s\neq 0} = 0 \qquad [w(y)\equiv 1] \qquad (15b)$$

The given downwash coefficients w_s and the unknown coefficients $C_{2\lambda+1}$ of (2) are interrelated by the infinite linear system

$$w_s = \pi\sum_{\lambda=0}^{\infty} c_\lambda{}^s C_{2\lambda+1} = \pi C_{2s+1} - \frac{1}{\pi}\sum_{\lambda=0}^{\infty}\bar{c}_\lambda{}^s C_{2\lambda+1} \qquad (16)$$

The matrix $c_\lambda{}^s$ is almost the unit matrix; the numbers $\bar{c}_\lambda{}^s$ are small (see Table 4).

Table 2 Values of $c_\lambda{}^s$

	λ			
s	0	1	2	3
0	*0.9112*	−0.0470	−0.0315	−0.0236
1	−0.0117	*0.9902*	−0.0078	−0.0064
2	−0.0039	−0.0041	*0.9964*	−0.0032
3	−0.0018	−0.0021	−0.0021	*0.9981*

The $\bar{c}_\lambda{}^s$ values are determined by the formulas

$$\bar{c}_\lambda{}^s = MS-(M-N)L_{s,\lambda} \quad \text{if } \lambda\neq s$$
$$= T-[4\bar{s}/(4\bar{s}+1)]S \quad \text{if } \lambda = s \qquad (16a)$$

where

$$M = \bar{\lambda}/(\bar{\lambda}^2-(s+1)^2); \qquad N = \bar{\lambda}/(\bar{\lambda}^2-\bar{s}^2)$$
$$L(s,\lambda) = 2L_\lambda+(1/2\bar{\lambda})-(1/2\bar{s})-2L_s$$
$$S = 2\log 2-\sum_{\nu=1}^{s}\frac{1}{(2\nu-1)\nu}-\frac{1}{2(2s+1)(s+1)} \qquad (16b)$$
$$T = \frac{\pi^2}{4}-\sum_{\nu=1}^{s}\frac{2}{(2\nu-1)^2}-\frac{1}{(2s+1)^2}$$
$$L_s = \sum_{\nu=1}^{s}\frac{1}{2\nu-1}(\sim\tfrac{1}{2}\log s)$$

and $\bar{s}\equiv(s+\frac{1}{2})$ corresponds to $\bar{\lambda}$ in Eqs. (6a) and (6b).

An alternative to the linear system (16) is the system

$$w_s = 2\sum_{\kappa=0}^{\infty} b_\kappa{}^s C_{2\kappa} \qquad (17)$$

where

$$4b^s = 1/(\kappa+\bar{s})+1/(\kappa+s+1)-2/(\kappa-\bar{s})$$

This is the simplified form of the original Kinner system; it has been used to derive the analytical result (7). For numerical work, the system (16) is preferred because it converges faster; this is because the $C_{2\lambda+1}$ converge faster than the $C_{2\kappa}$ [compare (7) and (11)].

3. Numerical Results

a. The Planar Solution

Ordinarily, in order to obtain the sets $C_{2\kappa}$ and $C_{2\lambda+1}$ for a given set w_s [from (15)], one truncates the linear system (16) to N equations, solves this and obtains an approximate truncated set $C_{2\lambda+1}{}^N$. Using this set in (6b), one obtains an approximate truncated set $C_{2\kappa}{}^N$. The complete procedure is programmed readily for digital computation. In our computer program, N is an open parameter. The results converge rapidly, as N is increased, as long as N is fairly small; unfortunately, they converge with increasing slowness when N becomes larger [this was to be expected from (11)]. However, already at $N = 40$ one obtains an accuracy of about 10^{-7} in $C_{2\lambda+1}$, and in $C_{2\kappa}$ for smaller κ. Toward the tail end of the set $C_{2\kappa}$, the accuracy decreases to 10^{-6}. (These accuracies apply to the reference problem (15b); the accuracy goes down, of course, or N has to be increased, if higher nonzero w_s occur.) For most purposes, one obtains ample accuracy with $N = 40$ over the inner part of the wing. In order to match with analytical results, (10) and (14), near the tip, one needs also the amplitude a_2. This is obtained from (7) by assuming that $R_\kappa = 0$ for the highest $C_{2\kappa}{}^N$.

We have determined the planar solution, our reference solution, plus three other solutions to very high accuracy in order to demonstrate definitely the analytical structure of the solutions and the power of the available methods. We used up to $N=60$ equations, used 12 decimals in the results to extrapolate to $N = \infty$, lost 2 decimals in the extrapolations, and performed the further calculations with 10 decimals.

The calculation of additional accurate solutions becomes easier once a reference solution has been determined. First, let us discuss the reference solution, which is denoted by the suffix 0 in Table 3. Details of the extrapolation procedure are given in Ref. 6. The amplitude a_2 was determined by means of Eqs. (4) and (8); in the extrapolation to $N = \infty$, use was made of the fact that the leading set of $C_{2\lambda+1}$ has the factor a_2, see (11), and that the next is $O(1/\lambda^3)$. This procedure also is described in Ref. 6.

Table 3 lists $C_{2\kappa,0}$, rounded off to 8 decimals, up to $\kappa = 15$, and lists the remainder R_κ which was calculated by means of the listed value a_2. For better visibility, the columns of numerical results, $C_{2\kappa,0}$ etc., have been multiplied by 10^8 in Tables 3 and 4. The remainder R_κ is broken down further in the manner shown [L_κ is the logarithmic set defined in (6b)], and a final remainder

Table 3 Planar solution $[w(y) \equiv 1]$

κ	$C_{2\kappa,0}$	R_κ	$\bar{R}_\kappa$
0	+22375288	−4654659	+184543
1	−14455778	+4313858	−148142
2	− 3065010	+ 255042	− 30011
3	− 1349032	+ 52375	− 4664
4	− 761010	+ 17088	− 1125
5	− 489108	+ 7158	− 355
6	− 340778	+ 3510	− 134
7	− 251341	+ 1919	− 57
8	− 192964	+ 1137	− 27
9	− 152820	+ 716	− 13
10	− 124027	+ 473	− 7
11	− 102674	+ 325	− 4
12	− 86400	+ 231	− 2
13	− 73712	+ 168	− 1
14	− 63628	+ 125	− 1
15	− 55481	+ 96	$(\kappa \geqq 15)$ 0

$\times 10^{-8}$

$$-C_{2\kappa,0} = \left[\frac{4}{\kappa(4\kappa+1)} - \frac{3\log^2\kappa}{16\pi^2\kappa^4}\right] a_2 + R_\kappa$$

$$R_\kappa = (1/\kappa^4)(b_4 L_\kappa + c_4) + \bar{R}_\kappa$$

$$a_2 = 0.1267740, \quad b_4 = 0.0029655, \quad c_4 = 0.0416545$$

$\bar{R}_\kappa$ is listed in the last column. This column is zero (to 8 decimals) from $\kappa = 15$ onward.

The constants b_4 and c_4 were determined by means of the three conditions

$$\text{a)}\ \ \bar{R}_p = 0; \qquad \text{b)}\ \ \sum_0^p \bar{R}_\kappa = 0; \qquad \text{c)}\ \ \bar{R}_\kappa = 0 \text{ for } \kappa > p \tag{18}$$

Here p is a number which has to be determined by trial and error. One chooses p and determines b_4 and c_4, using conditions a and b. The zero sum condition (5) must apply to the set $\bar{R}_\kappa$ (that is, if both analysis and numerical work are without error) because it applies individually to all other sets in $C_{2\kappa}$. Hence the sum of all $\bar{R}_\kappa$ from $(p+1)$ to ∞ must be zero when b is fulfilled. However, this does not insure that c is fulfilled. Rather, if p is too small, the $\bar{R}_\kappa$ beyond p describe a wavy curve about the zero line.

On the other hand, significant decimals are lost, and the constants b_4 and c_4 will be ill-defined if p is chosen too large. In fact, it is not possible to determine these constants very accurately; although 7 decimals are listed in Table 3, the last decimals should not be considered reliable. A small change in b_4 and c_4 will affect the first few listed values $\bar{R}_\kappa$; however, since these first few values almost cancel each other, the changes will cancel out entirely, and the validity of Eqs. (18) will not be affected.

That it was possible to find p, b_4, and c_4 such that (18) was fulfilled to 10 decimals (allowing for rounding-off errors), and the set $\bar{R}_\kappa$ converged smoothly and rapidly: this fact can be considered an over-all confirmation of the validity of analysis and numerical work. (We used $p = 20$.)

The set $C_{2\kappa,0}$ converges slowly; written out to 8 decimals it would extend to about $\kappa = 5000$. Table 3 demonstrates that, knowing the structure of the solution, one can store it in form of the short set $\bar{R}_\kappa$ plus the three numbers a_2, b_4, and c_4. (These numbers have to be treated as exact numbers, of course, when one uses them to reconstruct the set $C_{2\kappa,0}$.) The stored numbers then contain all the specific information about the specific solution; the bulk of the infinite set $C_{2\kappa,0}$ describes the general tip singularity. The number a_2 as listed in Table 3 is more reliable than b_4 and c_4. It determines the tip value of the lift coefficient; our estimate is that the value

Table 4 Void solutions $C_{2\kappa,nv}$ $(n = 1, 2, \text{and } 3) \times 10^{-8}$

κ	$C_{2\kappa,1v}$	$\bar{H}_\kappa$	$C_{2\kappa,2v}$	$\bar{H}_\kappa$	$C_{2\kappa,3v}$	$\bar{H}_\kappa$
0	−8355512	+20721931	−5930407	+30776604	−4502880	+43750001
1	+10240765	−21639945	+4670161	−27618971	+3210567	−39520727
2	− 1601144	+ 870664	+2349934	− 3789344	+ 938151	− 3174875
3	− 186437	+ 40008	− 856274	+ 571340	+1056414	− 1494365
4	− 52361	+ 5546	− 137425	+ 47133	− 519578	+ 381883
5	− 20553	+ 1224	− 46234	+ 9207	− 98681	+ 42559
6	− 9737	+ 355	− 20422	+ 2548	− 37073	+ 10118
7	− 5216	+ 124	− 10521	+ 865	− 17716	+ 3217
8	− 3048	+ 49	− 6001	+ 337	− 9684	+ 1211
9	− 1902	+ 22	− 3683	+ 145	− 5786	+ 510
10	− 1248	+ 10	− 2389	+ 67	− 3686	+ 233
11	− 854	+ 5	− 1620	+ 33	− 2466	+ 113
12	− 604	+ 3	− 1138	+ 17	− 1716	+ 57
13	− 439	+ 2	− 823	+ 9	− 1232	+ 30
14	− 327	+ 1	− 610	+ 5	− 908	+ 16
15	− 249	+ 1	− 462	+ 3	− 685	+ 9
16	− 192	$(\kappa \geqq 16)$ 0	− 357	+ 1	− 526	+ 5
17			− 280	+ 1	− 411	+ 3
18			− 222	$(\kappa \geqq 18)$ 0	− 326	+ 1
19					− 262	+ 1
20					− 213	$(\kappa \geqq 20)$ 0
a_2	= 0		= 0		= 0	
b_4	= 0.0086548		= 0.0024522		= −0.0156775	
c_4	= 0.1053370		= 0.2270359		= 0.3787791	

$w_{1,v}(y) = (5y^2-1)/4 - 0.4324159$
$w_{2,v}(y) = (21y^4-14y^2+1)/8 - 0.2795066$
$w_{3,v}(y) = (429y^6-495y^4+135y^2-5)/64 - 0.20268387$

$$C_{l,0}(1) \approx 1.593089 \tag{19}$$

should be reliable to about one unit in the last decimal given.

We close this section by noting also the values $C_{L,0}$ and $\xi_{L,0}$ which arise by means of (3e). For these, a fair number of approximate results are given in the literature. Our results

$$C_{L,0} \approx 1.79002303; \quad -\xi_{L,0} \approx 0.52085758 \tag{20}$$

should be reliable to less than one unit in the last decimal given.

b. Additional Solutions

As mentioned earlier, the calculation of additional accurate solutions becomes easier once a reference solution is available. Replace (7) by

$$-C_{2\kappa} = -XC_{2\kappa,0} + H_\kappa \tag{21}$$

and determine X such that $a_2 = Xa_{2,0}$. The set H_κ then converges $O(\kappa^{-4}\log\kappa)$, just as the remainder set R_κ in (7); but, while R_κ contains higher order sets which have the factor a_2, all such sets have been eliminated from H_κ. Hence H_κ can be called a void set; alternatively, one can call H_κ that specific signature of the given downwash $w(y)$ which distinguishes $C_{2\kappa}$ from $C_{2\kappa,0}$.

The main advantage of using Eq. (21) is that it is easier to determine X than it is to determine a_2 directly. In practice, one calculates simultaneously $C_{2\lambda+1,0}{}^N$ and $C_{2\lambda+1}{}^N$ and determines X such that the difference is free of the leading terms. Again, details are given in Ref. 6.

The results for three downwash distributions $w_n(y)$ are listed in Table 4 in the form corresponding to Table 3

$$-C_{2\kappa,nv} = H_\kappa = (1/\kappa^4)(b_4 L_\kappa + c_4) + \bar{H}_\kappa \tag{22}$$

The subscript v denotes the void part of this solution.

A logical choice for the $w_n(y)$ are the Gegenbauer polynomials

$$w_n(y) = \bar{P}_{2n}(y) \tag{23}$$

The corresponding downwash coefficients w_s are from (15a)

$$w_{n,n} = [(n+1)(2n+1)]^{-1}; \qquad w_{s,n} = 0 \quad \text{for} \quad s \neq n \tag{23a}$$

Our reference solution fits into this sequence as the case $n = 0$. If one stores the solutions for a number of these w_n, one can compose the members of a class of solutions as required. Table 4 lists the solutions for $n = 1$, 2 and 3. The downwash $w_n(y)$ is given in Table 4 in the form

$$w_{n,v}(y) = w_n(y) - X_n \tag{24}$$

The complete solution $C_{2\kappa,n}$ is given by

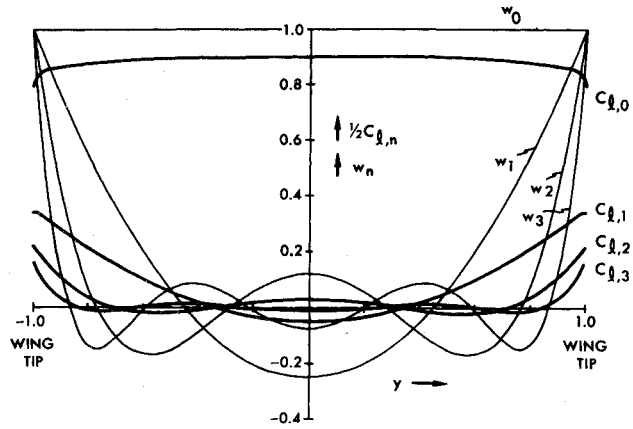

Fig. 5 Span loadings $C_{l,n}(y)$.

$$C_{2\kappa,n} = X_n C_{2\kappa,0} + C_{2\kappa,nv} \tag{25}$$

There is a sign change between $\kappa = n$ and $\kappa = n+1$ in the columns of Table 4. The numerical values in the sets $\bar{H}_\kappa$ increase as n increases, and consequently the listed sets become longer.

By definition, the curves of the void lift coefficients $C_{l,nv}(y)$ go to zero at the tip. Apparently they have a finite tip tangent.

4. Discussion of Results

An observation of physical interest is the following: one can form the ratio between two integrals over the wing, the total lift and the integral over the downwash momentum. This ratio is almost invariant between the reference solution and the three void solutions, Table 4; the maximum variation is less than 1%. With respect to total lift, it appears that the details of how the downwash is distributed over the wing span are of negligible importance and do not affect the outer flow (which determines the total lift).

The same ratio varies somewhat more when the complete solutions $C_{2\kappa,n}$ are compared. This is due to small differences between large numbers in (21) when these solutions are composed. With the complete solutions, the lift-momentum ratio varies from 0.895 for $n = 0$ to 0.821 for $n = 3$.

The complete solutions are shown in Fig. 5, both the given downwash distributions $w(y)$ and the resulting lift coefficient distributions $C_{l,n}(y)$. All the latter curves form a downward hook on approaching the wing tip and reach a vertical tangent at the tip itself. However, on the scale of Fig. 5, this hook no longer is visible when $n = 2$; even though the bulk of the set $C_{2\kappa}$ still represents the tip singularity, the latter now plays a minor role in the span loading curve.

The scale ratio between w_n and $C_{l,n}$ in Fig. 5 is chosen so that w_0 and $C_{l,0}$ have roughly the same over-all magnitude. For $n \neq 0$, the curves are wavy, and the wave amplitudes in $C_{l,n}$ are seen to be distinctly smaller than the corresponding amplitudes in w_n. Each amplitude ratio corresponds roughly to the ratio between half-wavelength and wing span. This is what one would expect from either lifting line theory or slender wing theory (according to either, the lift coefficient becomes proportional to the aspect ratio when the latter becomes sufficiently small), assuming that one can interpret the length of a half-wave as an effective wing span. That one can do this (roughly) is not entirely unexpected, but it is of interest to see the point verified.

Lifting line theory overpredicts (at small aspect ratios) by a factor of 2. This is illustrated for $n = 3$ in Fig. 6. Thus, Fig. 6 implies that the correct result corresponds closely to what we would expect from slender wing theory for $n = 3$. On the other hand, no slender wing analysis is available for the case $n = 3$. A collocation analysis for $n = 3$ would be feasible but rather cumbersome and would not necessarily be considered reliable.

How many chordwise modes would one have to use with spanwise waves this short? An indication of the answer is provided by Fig. 7, where, as in Fig. 2, a relief diagram of $\bar{p}$ is shown, here for $n = 3$. The left half of the wing is shown to exhibit the wavy distribution of the wing incidence. Again, the relief is shown over the right half-wing; however, in Fig. 7, this half-wing is stretched into a rectangle to facilitate observation of $\bar{p}$. Furthermore, the rectangle is cut at $y = 0.9$. The finite chord at the wing tip, produced by the stretching operation, exhibits the kinked-linear character of the chordwise distribution at the tip. Part of a vertical plane through the stretched leading edge is shown by a line of constant $\bar{p}$ (the scale of $\bar{p}$ is arbitrary) and by vertical lines of constant y.

The most striking insight of technical interest from Fig. 7 is that although the waviness of $w(y)$ is well reflected in $\bar{p}_{\text{l.e.}}$, it has

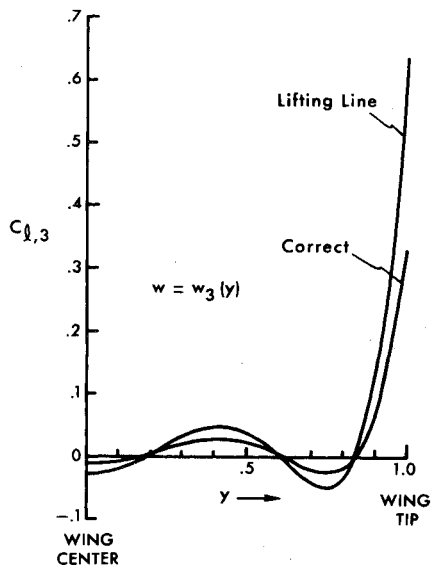

Fig. 6 Comparison of lifting line result with exact solution.

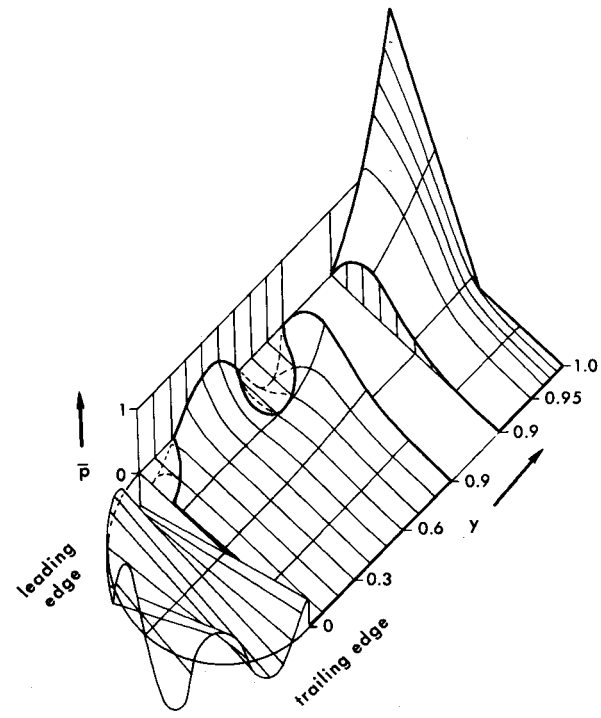

Fig. 7 Pressure function for $n = 3$.

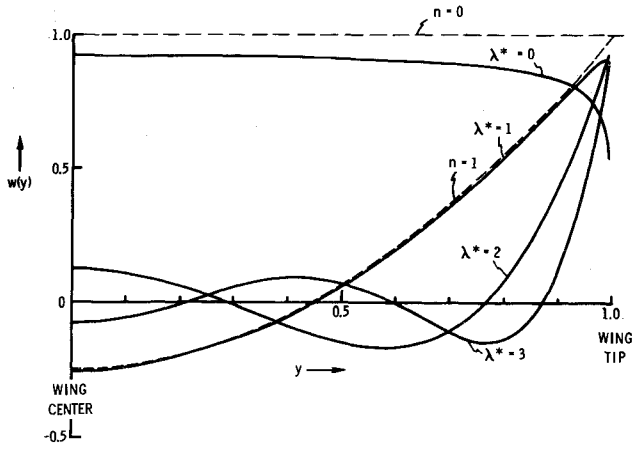

Fig. 8 Elementary downwash distributions.

disappeared completely over the rear part of the wing. This stabilizing effect, the cause for the smaller magnitude of the wave amplitudes in $C_{l,3}$ in Figs. 5 and 6, is of considerable interest; although it is shown here for idealized models, it must be of significance for the influence of any disturbances of short spanwise extension.

The chordwise distributions of $\bar{p}$ in Fig. 7 are not kinked (except, of course, at the tip itself) but they are fairly complicated curves. For the planar circular wing ($n = 0$) two Birnbaum-Glauert chordwise modes are sufficient to yield an excellent approximation.[9] For the case $n = 3$, only two modes (i.e., approximation by a parabola) clearly would be insufficient.

The difference between the complex distribution in Fig. 7 and the reference distribution in Fig. 2 is contained in the rapidly converging void set $C_{2\kappa,3v}$, Table 4. The tip singularity is common to both figures; it is described by the bulk of the slowly converging complete set $C_{2\kappa}$, Table 3.

5. An Approximate Approach

The preceding discussions concentrated on the set $C_{2\kappa}$; for example, we used the rational sets (9) as some of its elements. One can define other elements from which to build up the solution for the given downwash $w(y)$. For example, choose an integer λ^* and let

$$C_{2\lambda^*+1} \neq 0; \qquad C_{2\lambda+1} = 0 \quad \text{for} \quad \lambda \neq \lambda^* \tag{26}$$

The pressure distribution which results by means of (6b) and (2) is characterized by its l.e. distribution

$$\bar{p}_{\text{l.e.}} = 8[\sin(2\lambda^*+1)\phi/\sin\phi]C_{2\lambda^*+1} \tag{26a}$$

It is a spanwise wavy distribution similar to that seen in Fig. 7.

In fact, two elements, n of (23) and λ^* of (26), are quite similar if $\lambda^* = n$ (except when $n = 0$). We set $\pi C_{2\lambda^*+1} = w_{n,n}$, compare (23a); then two equal numbered elements differ only by the effect of the small numbers $\bar{c}_\lambda{}^s$ in (16). This effect is illustrated in Fig. 8. Shown are the downwash distributions which belong to the first four elements λ^* [calculated by means of (15a)]. They all turn down to $w(1) = -\infty$ at the tip. Thus, none of these elements is, by itself, a technically meaningful solution; however, the downturn occurs closer and closer to the tip as λ^* increases. Because of this, a finite tip value $w(1)$ (and thus a technically meaningful solution) can be built up with an infinite number of elements λ^*. Shown as dashed lines in Fig. 8 are the corresponding downwash distributions (Gegenbauer polynomials) $w_n(y)$. There is a sizable difference between the full and the dashed lines for $n = 0$, but only a very small difference for $n = 1$ (except at the tip). No visible difference remains when $n = 2$ or $n = 3$.

In view of the fact that two corresponding elements become increasingly close to being identical, one cannot, on the scale of Fig. 7, determine if this drawing represents the case $n = 3$ or the case $\lambda^* = 3$. To be sure, the tip values $w(1)$ always differ (being 1 and $-\infty$, respectively), but this difference in $w(1)$ produces a difference of only 1.4% in $C_l(1)$ when $n = \lambda^* = 3$.

The elements λ^* are very convenient. One needs only the transformation (6b); no linear system has to be solved. For many purposes (for example, in an investigation of the effect of a local disturbance or a discontinuity in $w(y)$ on the inner part of the wing span) one can use Tables 1 and 2 for $n = 0$ to 3 and can use the λ^* for all larger n.

6. Conclusion

The nature of the pressure singularity at a parabolic wing tip is now known, and all required details of the analytical structure of exact solutions for circular wings are at hand. Therefore, it has become possible to use numerical results with confidence. One knows their convergence behavior and can match with the asymptotic wing tip solution. The procedure for calculating numerical solutions for the circular wing has been described (limited, so far, to symmetric downwash distributions without camber, but generalization is possible).

Four sample solutions have been calculated to very high accuracy and have been tabulated. The solving sets converge slowly; their bulk, typified by the solution for the planar wing, describes the tip singularity. This singularity can be split off; the specific solutions which remain are void of the tip singularity and converge rapidly. The sample solutions exhibit details of the mechanism of lifting flow and are of technical interest.

The numerical technique described in this paper allows one to investigate, for example, the pressure distribution arising from a local distribution or a discontinuity in the downwash. In such a problem, the quick approximation method of Sec. 5 may be useful; approximation becomes increasingly accurate with higher order effects, and its analytical simplicity may allow analytical treatment of the given problem.

References

[1] Kinner, W., "Die kreisförmige Tragfläche auf potentialtheoretischer Grundlage," *Ingenieur-Archiv*, Vol. 8, No. 1, Feb. 1937, pp. 47–80.

[2] Jordan, P. F., "The Parabolic Wing Tip in Subsonic Flow," AIAA Paper 71-10, San Diego, Calif., 1971; also AFOSR-TR-71-0075, 1971, Air Force Office of Scientific Research, Arlington, Va.

[3] Jordan, P. F., "Span Loading and Wake Formation," *Aircraft Wake Turbulence and its Detection*, Plenum Press, New York, 1971, pp. 207–227.

[4] Jordan, P. F., "On Lifting Wings with Parabolic Tips," RIAS TR 72-16c, July 1972, Martin Marietta Labs., Baltimore, Md.; also AFOSR-TR-72-1738, 1972, Air Force Office of Scientific Research, Arlington, Va.

[5] Jordan, P. F., "A Reversible Transformation and Related Sets of Legendre Coefficients," RIAS TR 72-14c, July 1972, Martin Marietta Labs., Baltimore, Md.; also AFOSR-TR-1706, 1972, Air Force Office of Scientific Research, Arlington, Va.

[6] Jordan, P. F., "Exact Solutions for Lifting Surfaces," RIAS TR 72-17c, Aug. 1972, Martin Marietta Labs., Baltimore, Md.; also AFOSR TR-72-1737, 1972, Air Force Office of Scientific Research, Arlington, Va.

[7] Abramowitz, M. and Stegun, I. A., eds., *Handbook of Mathematical Functions*, 3rd printing, National Bureau of Standards, Washington, D.C., 1965.

[8] Zandbergen, P. J., Labrujere, T. E., and Wouters, J. G., "A New Approach to the Numerical Solution of the Equation of Subsonic Lifting Surface Theory," NLR TR G. 49, Nov. 1967, National Lucht-en Ruimtevaart-laboratorium, The Netherlands.

[9] Jordan, P. F., "Remarks on Applied Lifting Surface Theory," *Jahrbuch 1967 der WGLR*, 1968, pp. 192–210.